J Porous Mater (2015) 22:629–634
DOI 10.1007/s10934-015-9935-7

SO_3H-functionalized hollow mesoporous carbon sphere prepared by simultaneously achieving sulfonation and hollow structure

Binbin Chang[1] · Yanchun Li[1] · Yanzhen Guo[1] · Hang Yin[1] · Shouren Zhang[1] · Baocheng Yang[1]

Published online: 10 March 2015

Abstract SO_3H-functionalized hollow mesoporous carbon sphere (HMCS–SO_3H) was successfully synthesized via a facile strategy using inexpensive resins as precursor in combination with metal oxide template. By the one-step thermal treatment with sulfuric acid, it simultaneously achieved the formation of hollow spherical structure and sulfonation functionalization. HMCS–SO_3H catalyst possessed superior mesoporosity, uniform sphere morphology and high acidity, which endowed it excellently catalytic property for esterification of oleic acid. In addition, HMCS–SO_3H exhibited prominent stability and reusability.

Keywords Carbon materials · Mesoporous · Hollow sphere · Sulfonation

1 Introduction

Carbon-base solid acids were regard as an ideal heterogeneous acid for many reactions, and thus have received much attention for their advantages, such as chemical inertness, high mechanical stability, low cost, structural diversity and high chemical activity. Traditionally, carbon-base solid acid can be readily prepared by incomplete carbonization of sulfopolycyclic aromatic compounds in conc. H_2SO_4 or sulfonation of incompletely carbonized natural organic matter [1, 2]. However, these SO_3H-bearing carbon-base acids usually possess low surface area and poor porosity, which strongly restrict the interaction between acidic active sites and substrates. Subsequently, sulfonated mesoporous carbon solid acids with high surface area and superior porosity were obtained via different strategies. Liu et al. [3] prepared sulfonated ordered mesoporous carbon acids by a hard-template method with an acidity of 1.95 mmol H^+ g^{-1} and satisfactory catalytic performance. We also prepared sulfonated mesoporous carbon solid acid catalyst with a higher acidity of 2.09 mmol H^+ g^{-1} and impressive catalytic activity by a soft-template route [4].

Although these sulfonated mesoporous carbon acids exhibit prominent porosity and high acidity, their catalytic property still have much space of improvement [5–7]. Considering the structural diversity of carbon materials, carbon-base solid acids with various morphology and structure were synthesized to further enhance the catalytic performance, such as nanoparticle, nanosheet, nanosphere and hollow sphere. Among them, hollow carbon nanosphere, especially hollow porous carbon sphere materials, have received considerable attention for application in catalysis, owing to their low density, high accessible surface area, controllable inner pore volume and uniform structure [8, 9]. Various approaches have been developed for preparing carbon-base solid acids with hollow structure and superior porosity. The major class of synthesis methods is the hard template method, which need the fabrication of core–shell templates and the subsequent removal of these templates and the final functionalization of sulfonation. For example, Wang et al. [10] have synthesized sulfonated hollow sphere carbon with using the SiO_2 core as template and sulfonation with chlorosulfonic acid. Apparently, this route is a typical multi-step and time-consuming process.

✉ Binbin Chang
binbinchang@hotmail.com

✉ Baocheng Yang
baochengyang@yahoo.com

[1] Institute of Nanostructured Functional Materials, Huanghe Science and Technology College, Zhengzhou 450006, Henan, China

Herein, we demonstrate a successful synthesis of SO_3H-functionalized hollow mesoporous carbon sphere (HMCS–SO_3H) solid acid by simultaneous achievement of sulfonation and hollow spherical structure formation.

2 Experimental section

2.1 Materials synthesis

The dispersible Fe_3O_4 nanospheres and Fe_3O_4@MC core–shell structure material were prepared according to the route reported previously [11, 12]. Following, 1 g of Fe_3O_4@MC material was mixed with 20 mL of sulfuric acid, and then the mixed solution was placed in a Teflon–sealed autoclave and maintained at 180 °C for 8 h. Finally, the black powder were washed repeatedly with hot distilled water (>80 °C) until the sulfate ions were no longer detected in the wash water ($BaCl_2$ precipitation test) and were dried at 80 °C for 6 h. The resulting materials were denoted as HMCS–SO_3H.

2.2 Characterization

The X-ray diffraction (XRD) patterns of powder samples were taken by a Bruker D8 Advance diffractometer using Cu Kα radiation (λ = 0.15418 nm) as an X-ray source. N_2 adsorption–desorption isotherms were carried out at −196 °C using a micromeritics ASAP 2020 analyzer. The specific surface area (S_{BET}) was evaluated using the Brunauer–Emmett–Teller (BET) method. The pore size distributions were calculated according to the Barrett–Joyner–Halenda (BJH) formula applied to the adsorption branch. Fourier transform infrared spectroscopy (FTIR) spectra of a sample in KBr pellet were recorded on a Thermo scientific Nicolet IS5 spectrometer. The morphology was observed from a FEI Tecnai G2 20 transmission electron microscope (TEM) with an accelerating voltage of 200 kV and a scanning electron microscope (SEM, Quanta 250 FEG).

2.3 Catalytic test

The catalytic property of HMCS–SO_3H material was evaluated by the esterification of oleic acid with methanol. Typically, 0.005 mol of oleic acid (OA) was mixed in anhydrous methanol (MeOH) in the round bottom flask and the fixed mass of catalyst (30 mg) was added. After the finish of reaction, the samples were centrifuged to separate the catalyst powder, and then the methanol and water were evaporated out of the samples, and the product analyzed for acid value by titration [13]. The conversion of oleic acid was calculated using the following formula:

$$\text{Conversion}\,\% = (1 - \text{AV}_x/\text{AV}_0) \times 100\,\%$$

where AV_x is the instant acid value of samples drawn from the reaction mixture, AV_0 is the initial acid value of oleic acid.

3 Result and discussion

XRD patterns of Fe_3O_4, Fe_3O_4@MC and HMCS–SO_3H are shown in Fig. 1 to demonstrate the evolution of material structure. The characteristic diffraction peaks of Fe_3O_4 are present in Fe_3O_4 and Fe_3O_4@MC samples, which can be assigned to the (111), (220), (311), (222), (400), (422), (511) and (440) planes of a pure cubic Fe_3O_4 phase (JCPDS no. 19-629). No evident differences were found between Fe_3O_4 and Fe_3O_4@MC. The grain size of Fe_3O_4 in Fe_3O_4@MC is roughly calculated to be 31.24 nm, which is larger than 23.98 nm for the Fe_3O_4 sample, suggesting the improvement of crystallization during the process of further carbonization. After the functionalization of sulfonation, the characteristic diffraction peaks of Fe_3O_4 disappeared, suggesting the successful removal of magnetic core. The weak and broad different peak at about $2\theta = 20°–30°$ in HMCS–SO_3H sample should be caused by the amorphous carbon, which verified the successful coating of carbon layer onto the magnetic core. The EDS spectra of Fe_3O_4@MC and HMCS–SO_3H samples are displayed in Fig. 2, and further confirm their compositions of as-synthesized materials. As shown in Fig. 2a, the signal of C element exists in the Fe_3O_4@MC sample, which also testified the successful coating of carbon shell. After thermal treatment with concentrated sulfuric acid, the signal of S element appears in HMCS–SO_3H sample,

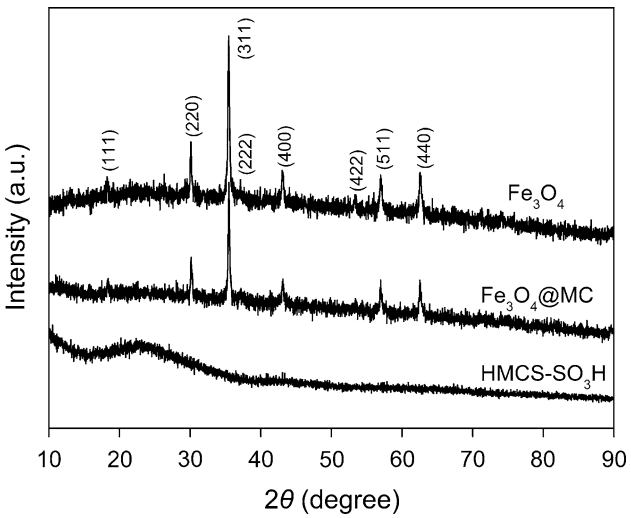

Fig. 1 The large-angel XRD patterns of Fe_3O_4, Fe_3O_4@MC and HMCS–SO_3H

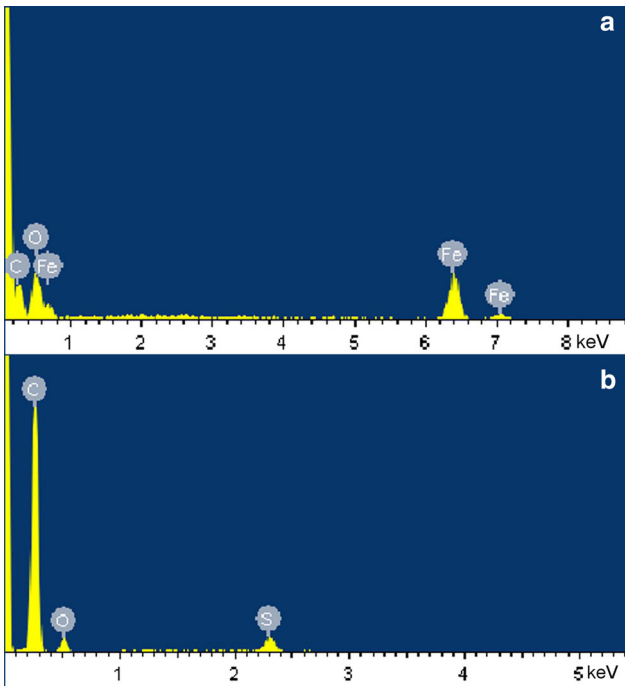

Fig. 2 The EDS spectra of Fe_3O_4@MC and HMCS–SO_3H samples

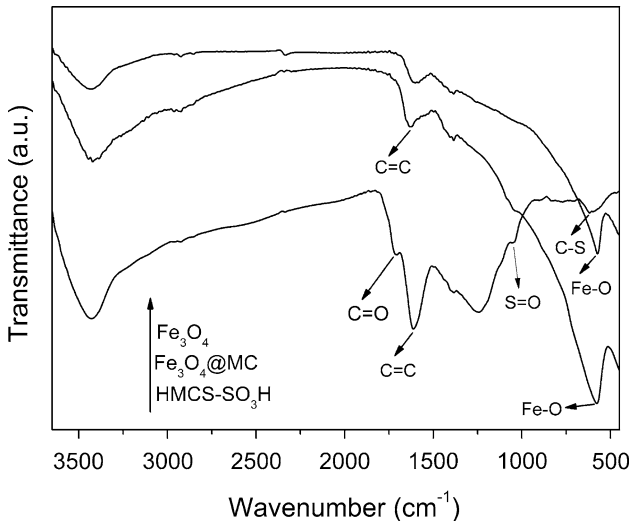

Fig. 3 FTIR spectra of Fe_3O_4, Fe_3O_4@MC and HMCS–SO_3H samples

indicative of the successful functionalization of sulfonation. Furthermore, the signal of Fe element disappears, suggesting the removal of Fe_3O_4 magnetic core. Consequently, the process of thermal treatment with sulfuric acid simultaneously achieves the functionalization of sulfonation and the formation of hollow structure.

To further identify the presence of functional groups and the successful removal of magnetic core, the FTIR spectra of Fe_3O_4, Fe_3O_4@MC and HMCS–SO_3H samples are shown in Fig. 3. The characteristic adsorption band of Fe–O centered at about 575 cm^{-1} could be found in Fe_3O_4 and Fe_3O_4@MC samples. The additional adsorption band appeared at 1640 cm^{-1} in Fe_3O_4@MC should be related to the C=C stretching vibration, verifying the formation of carbon layer. In HMCS–SO_3H samples, the new adsorption band located at 1045 cm^{-1} should be attributed to the symmetric stretching vibrations of S=O [14], and another additional adsorption band at 620 cm^{-1} is ascribed to the bending vibration of –OH groups hydrogen bonded to –SO_3H group [15]. Meanwhile, the adsorption band of Fe–O is indiscoverable in HMCS–SO_3H samples. These results also demonstrate the simultaneity of sulfonation and the formation of hollow structure during the process of thermal treatment with sulfuric acid.

Electron microscope photographs were characterized to reveal the morphology and structure of samples. SEM and TEM images are shown in Figs. 4 and 5, respectively. As shown in SEM images, Fe_3O_4 nanoparticles display the uniform spherical structure, and the carbon layer can be clearly found in Fe_3O_4@MC sample. After thermal treatment, the HMCS–SO_3H sample shows a hollow sphere structure with average diameter of 400 ~ 600 nm, and some of spheres are partially broken, which more clearly display the hollow structure. TEM images more intuitively present the structure and morphology. Fe_3O_4@MC shows a typical core–shell structure, and the thickness of carbon shell is about 16 nm, and more importantly, the mesoporous structure of carbon shell is discernible (the insert Fig. 5b). After sulfonation, HMCS–SO_3H shows a superior and uniform sphere structure with an average diameter of ca. 500 nm hollow cavity.

To investigate the mesoporosity of materials, the nitrogen sorption isotherm and pore size distribution of materials are shown in Fig. 6. The sample of Fe_3O_4@MC exhibits a little adsorption of nitrogen, giving a very low surface area of about 58 $m^2\ g^{-1}$. However, HMCS–SO_3H sample shows a type IV sorption isotherm with a marked leap at relative pressure p/p_o from 0.45 to 0.90, which should associate with the N_2 filling of mesopores owing to the capillary condensation. Besides, this result also reflects the relatively large mesopore size existing in HMCS–SO_3H sample. The pore size distribution calculated from adsorption branches confirms a relatively large mesopore size at value of ~10.9 nm (Fig. 6b). Very interestingly, the specific surface area of HMCS–SO_3H is estimated at 280 $m^2\ g^{-1}$, which should be related to the removal of magnetic core during the process of sulfonation. The relatively large surface area is greatly helpful for promoting its catalytic performance.

The HMCS–SO_3H possesses uniform hollow structure and relatively high acidity, which should endow it excellently catalytic property for esterification of oleic acid. The

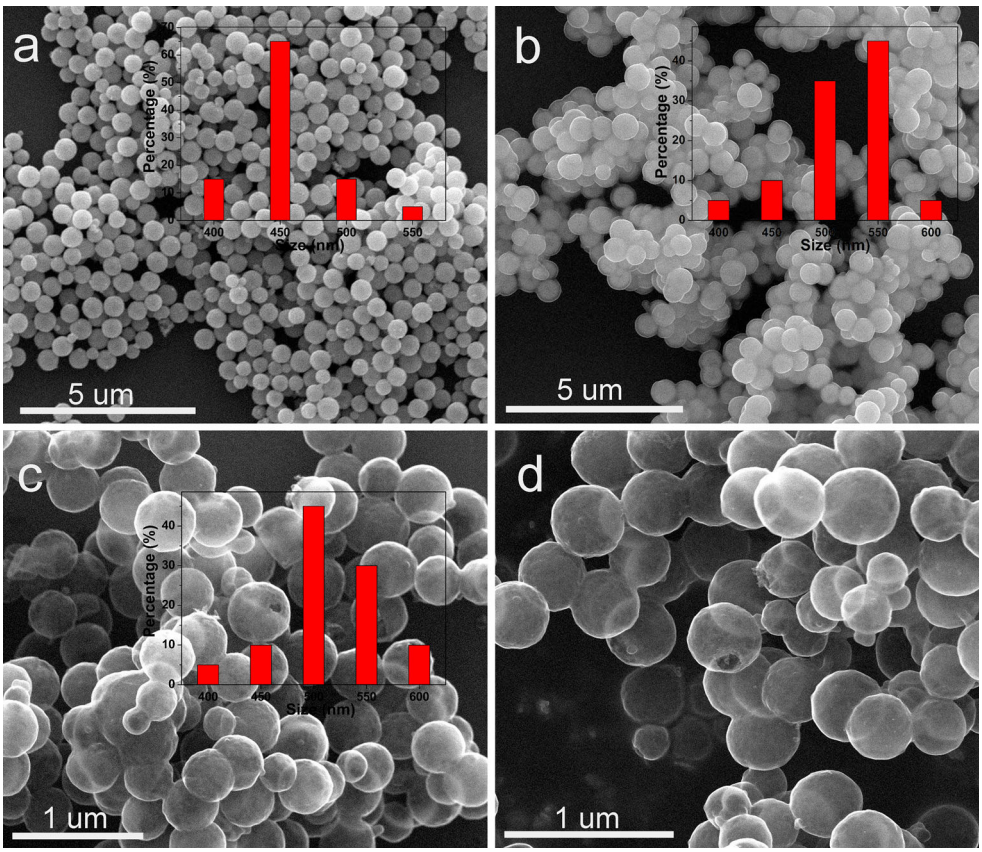

Fig. 4 SEM images of Fe_3O_4 (**a**), Fe_3O_4@MC (**b**) and HMCS–SO_3H (**c**, **d**) samples. *Insert* the corresponding particle size distributions for each sample

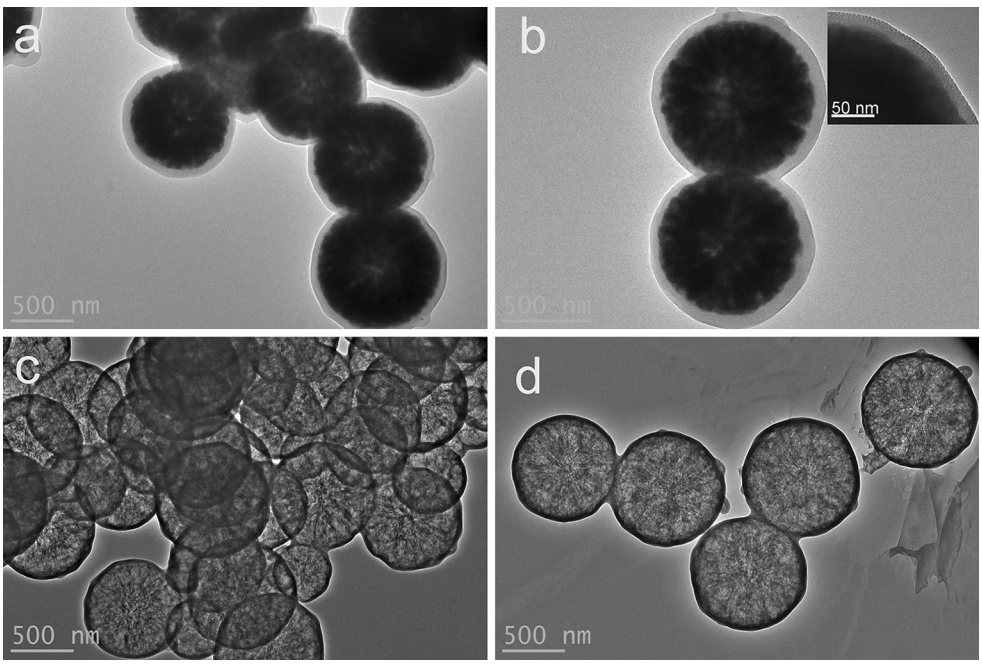

Fig. 5 TEM images of Fe_3O_4@MC (**a**, **b**) and HMCS–SO_3H (**c**, **d**) samples

catalytic activity of HMCS–SO_3H is shown in Table 1, and it is obvious that its performance is much better than those of other solid acid catalysts. As is well-known, reaction temperature and molar ratio of MeOH/OA have an important influence on the catalytic activity of solid acid. Consequently, in order to further evaluate the catalytic

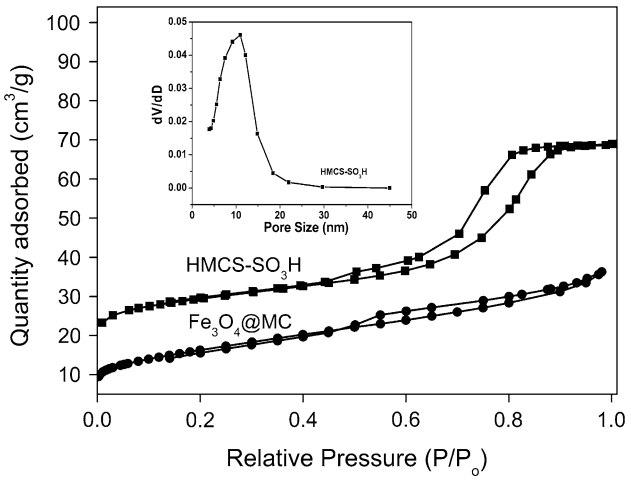

Fig. 6 N_2 adsorption–desorption isotherm of Fe_3O_4@MC and HMCS–SO_3H material, and the *insert* is the pore size distribution of HMCS–SO_3H

Table 1 The comparison of catalytic performance for esterification of oleic acid over HMCS–SO_3H and other catalysts reported in the literatures

Catalyst	Conversion (%)
HMCS–SO_3H[a]	93
OMC–H_2O_2–SO_3H[b]	76 [16]
OMC–150–SO_3H[c]	73 [3]
CMK-3–873–SO_3H[d]	55 [17]
SBA-15–ph-SO_3H[e]	49 [3]
Glu-Corn75[f]	85 [18]
CAT4[g]	50 [19]

Reaction conditions: [a] 2 wt% of catalyst, molar ratio = 10:1, 4 h, 70 °C; [b] 0.1 g of catalyst, molar ratio = 10:1, 2 h, 70 °C; [c] 50 mg of catalyst, molar ratio = 10:1, 10 h, 80 °C; [d] 0.1 g of catalyst, molar ratio = 10:1, 6 h, 80 °C; [e] 50 mg of catalyst, molar ratio = 10:1, 10 h, 80 °C; [f] 5 wt% of catalyst, molar ratio = 10:1, 4 h, 70 °C; [g] 7.5 wt% of catalyst, molar ratio = 60:1, 6 h, 65 °C

performance of HMCS–SO_3H, the influences of reaction temperature and molar ratio are displayed in Fig. 7. Under the different molar ratio, the influence of reaction temperature on the catalytic activity exhibits the same trend, whereby increasing the temperature enhances the OA conversion (Fig. 7a). When the temperature increases to 70 °C, the OA conversion reaches a highest value of above 94 % for 4 h at MeOH/OA molar ratio of 10:1, which should be ascribed to the high reaction temperature provides reactants and products with more energy, accelerating the mass transfer and thus raising reaction rate and conversion [16]. Further increasing reaction temperature to 80 °C, the conversion presents the tendency of decline, which should be caused from the higher temperature, resulting in the most of methanol stagnating in the refluxing. Esterification is a reversible reaction, so methanol is usually excessive to force the equilibrium to the direction of ester [20]. With the enhancement of MeOH/OA molar ratio, the conversion significantly increases (Fig. 7b). The low OA conversion of about 40 % was obtained with a MeOH/OA molar ratio of 1:1; however, the conversion was greatly improved under the 10:1 of molar ratio, and a ca. 93 % OA conversion was obtained. With the enhancement of methanol, the rate of forward reaction was sharply raised; meanwhile, the rate of reverse reaction was greatly restricted. Consequently, the increase of the MeOH/OA molar ratio contributes to drive the equilibrium to the ester side and bring a higher conversion. Further enhance the molar ratio of MeOH/OA, the speed of increase was slowed, which could be due to the reaction reaching the equilibrium state. The reusability of HMCS–SO_3H was depicted in Fig. 8. It was noteworthy to mention that the catalyst was reusable without any appreciable decrease in catalytic activity. After six consecutive cycles, the OA conversion could still reach above 94 %, suggesting its excellent reusability.

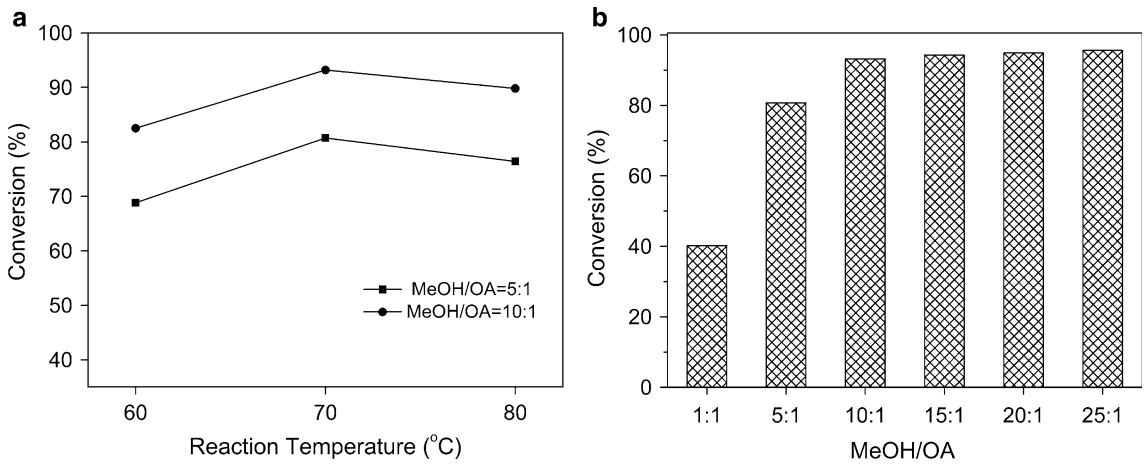

Fig. 7 The influence of reaction temperature (**a**) and MeOH/OA molar ratio (**b**) on catalytic activity of HMCS–SO_3H catalyst

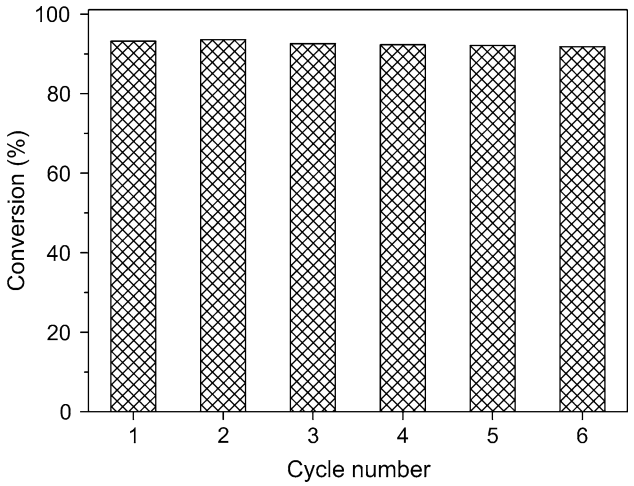

Fig. 8 The reusability of HMCS–SO_3H catalyst. (Reaction temperature 70 °C; MeOH/OA molar ratio = 10:1; Reaction time 4 h)

4 Conclusion

In conclusion, we have successfully prepared sulfonic group functionalized hollow mesoporous carbon sphere by simple and one-step thermal treatment with sulfuric acid. HMCS–SO_3H solid acid catalyst owns uniform hollow morphology, developed mesostructure and high SO_3H density. Meanwhile, the unique hollow sphere structure with superior mesoporosity favors it remarkable catalytic property for esterification of oleic acid, which is favorable for mass transfer in the reaction. More importantly, HMCS–SO_3H solid acid shows good catalytic stability and excellent recyclability. Furthermore, these features should be potentially important for design and synthesis of novel efficient carbon-base materials for many applications in catalysis, energy storage and conversion.

Acknowledgments The authors gratefully acknowledge the financial support from the program for New Century Excellent Talents in University (NCET-12-0696), the Leading Talents for Zhengzhou Science and Technology Bureau (Grant No. 131PLJRC649), the program for University Innovative Talents of Science and Technology in Henan Province (Grant No. 2012HASTIT03), National Natural Science Foundation of China (51472102).

References

1. M. Hara, Energy Environ. Sci. **3**, 601 (2010)
2. S. Suganuma, K. Nakajima, M. Kitano, D. Yamaguchi, H. Kato, S. Hayashi, M. Hara, J. Am. Chem. Soc. **130**, 12787 (2008)
3. R. Liu, X.Q. Wang, X. Zhao, P.Y. Feng, Carbon **46**, 1664 (2008)
4. B.B. Chang, J. Fu, Y.L. Tian, X.P. Dong, RSC Adv. **3**, 1987 (2013)
5. J. Tang, J. Liu, C.L. Li, Y.Q. Li, M.O. Tade, S. Dai, Y. Yamauchi, Angew. Chem. Int. Ed. **54**, 588 (2015)
6. J. Tang, J. Liu, N.L. Torad, T. Kimura, Y. Yamauchi, Nano Today **9**, 305 (2014)
7. J. Tang, N.L. Torad, R.R. Salunkhe, J.H. Yoon, M.S.A. Hossain, S.X. Dou, J.H. Kim, T. Kimura, Y. Yamauchi, Chem-Asian J. **9**, 3238 (2014)
8. Y.D. Xia, Z.X. Yang, R. Mokaya, J. Phys. Chem. B **108**, 19293 (2004)
9. B.B. Chang, W.W. Shi, D.X. Guan, Y.L. Wang, B.C. Zhou, X.P. Dong, Mater. Lett. **126**, 13 (2014)
10. L. Wang, J. Zhang, S. Yang, Q. Sun, L.F. Zhu, Q.M. Wu, H.Y. Zhang, X.J. Meng, F.S. Xiao, J. Mater. Chem. A **1**, 9422 (2013)
11. Y.F. Zhu, E. Kockkrick, T. Ikoma, N. Hanagata, S. Kaskel, Chem. Mater. **21**, 2547 (2009)
12. X.B. Zhang, H.W. Tong, S.M. Liu, G.P. Yong, Y.F. Guan, J. Mater. Chem. A **1**, 7488 (2013)
13. M. Hara, T. Yoshida, A. Takagaki, T. Takata, J.N. Kondo, K. Domen, S. Hayashi, Angew. Chem. Int. Ed. **43**, 2955 (2004)
14. B. Du, X. Zhang, L.L. Lou, Y.L. Dong, G.X. Liu, S.X. Liu, Appl. Surf. Sci. **258**, 7166 (2012)
15. B.R. Xing, N. Liu, Y.M. Liu, H.H. Wu, Y.W. Jiang, L. Chen, M.Y. He, P. Wu, Adv. Funct. Mater. **17**, 2455 (2007)
16. B.B. Chang, J. Fu, Y.L. Tian, X.P. Dong, J. Phys. Chem. C **117**, 6252 (2013)
17. L. Peng, A. Philippaerts, X.X. Ke, J.V. Noyen, F.D. Clippel, B.F. Sels, Catal. Today **150**, 140 (2010)
18. G. Chen, B.S. Fang, Bioresour. Technol. **102**, 2635 (2011)
19. B.V.S.K. Rao, K. Chandra Mouli, N. Rambabu, A.K. Dalai, R.B.N. Prasad, Catal. Commun. **14**, 20 (2011)
20. M.G. Kulkarni, R. Gopinath, L.C. Meher, A.K. Dalai, Green Chem. **8**, 1056 (2006)